

1 The authoritative version of this paper is available in the Elsevier journal *Science of the Total Environment*  
2 at: <http://dx.doi.org/10.1016/j.scitotenv.2012.01.046>

3  
4  
5 **Contaminant mobility and carbon sequestration downstream of the Ajka (Hungary)**  
6 **red mud spill: the effects of gypsum dosing**

7  
8 Renforth, P.<sup>1\*</sup>, Mayes, W.M.<sup>2</sup>, Jarvis, A.P.<sup>3</sup>, Burke, I.T.<sup>4</sup>, Manning, D.A.C.<sup>3</sup>, Gruiz, K.<sup>5</sup>

9  
10 <sup>1</sup> Department of Earth Sciences, University of Oxford, South Parks Road, Oxford, OX3  
11 ODP, UK

12 <sup>2</sup> Centre for Environmental and Marine Sciences, University of Hull, Scarborough, YO11  
13 3AZ, UK

14 <sup>3</sup> School of Civil Engineering and Geosciences, Newcastle University, Newcastle upon  
15 Tyne, NE1 7RU, UK

16 <sup>4</sup> School of Earth and Environment, University of Leeds, Leeds, LS2 9JT, UK

17 <sup>5</sup> Department of Applied Biotechnology and Food Science, Budapest University of  
18 Technology and Economics. 1111 Budapest, St. Gellért sq. 4. Hungary

19 \*Phil.Renforth@earth.ox.ac.uk

20  
21 **Abstract**

22 A number of emergency pollution management measures were enacted after the  
23 accidental release of caustic bauxite processing residue that occurred in Ajka, western  
24 Hungary in October, 2010. These centred on acid and gypsum dosing to reduce pH and  
25 minimise mobility of oxyanion contaminants mobile at high pH. This study assessed the  
26 effectiveness of gypsum dosing on contaminant mobility and carbon sequestration  
27 through assessment of red mud and gypsum-affected fluvial sediments via elemental  
28 analysis and stable isotope analysis. There was a modest uptake of contaminants (notably  
29 As, Cr, and Mn) on secondary carbonate-dominated deposits in reaches subjected to  
30 gypsum dosing. C and O stable isotope ratios of carbonate precipitates formed as a result  
31 of gypsum dosing were used to quantify the importance of the neutralisation process in

32 sequestering atmospheric carbon dioxide. This process was particularly pronounced at  
33 sites most affected by gypsum addition, where up to 36% of carbonate-C appears to be  
34 derived from atmospheric in-gassing of CO<sub>2</sub>. The site is discussed as a large scale  
35 analogue for potential remedial approaches and carbon sequestration technologies that  
36 could be applied to red mud slurries and other hyperalkaline wastes. The results of this  
37 work have substantial implications for the aluminium production industry in which 3-4%  
38 of the direct CO<sub>2</sub> emissions may be offset by carbonate precipitation. Furthermore,  
39 carbonation by gypsum addition may be important for contaminant remediation, also  
40 providing a physical stabilisation strategy for the numerous historic stockpiles of red  
41 mud.

42

43 **Keywords:** bauxite processing residue; red mud; carbon dioxide removal; stable isotope;  
44 hyperalkaline wastes; carbonate precipitation

45

## 46 **Introduction**

47 The failure of the north-western corner of Cell X of the Ajkai Timfoldgyar Zrt alumina  
48 plant's bauxite processing residue (red mud) depository on the 4<sup>th</sup> October 2010 led to a  
49 sudden release of 600,000-700,000m<sup>3</sup> of a highly caustic (pH 13) red mud suspension,  
50 which engulfed the downstream villages of Kolontár, Devecser and Somlóvásárhely in  
51 western Hungary (Gruiz, 2010; Mayes et al., 2011). The disaster prompted the activation  
52 of the EU Civil Protection Mechanism to combat the effects of the pollutant release.  
53 Immediate emergency management focussed on the removal of red mud from residential  
54 areas and in some cases the ploughing of thin surface deposits into underlying soils to  
55 minimise dust-blown hazards (Gruiz, 2010; Gelencsér et al., 2011). Water management  
56 initially focussed on neutralising pH through dosing with acid (acetic, hydrochloric,  
57 nitric) and gypsum throughout the Torna Creek and the Marcal and Rába rivers, prior to  
58 the outlet of the Rába system to the Danube. Water jets were used to aid gypsum mixing  
59 with high pH waters and were effective in limiting pH to levels below 10.5 in lower  
60 reaches of the Marcal River soon after the spill (Hungarian Ministry of Foreign Affairs,  
61 2010). Residual releases of red mud suspension from the breached cell were also a  
62 remedial priority, through the construction of a Permeable Reactive Barrier (PRB) from

63 the fly ash that previously comprised the wall, and of a series of settlement lagoons to  
64 minimise solids transport downstream from source zones (Gruiz, 2010; Mayes et al.,  
65 2011). Longer term efforts have seen a semi-permanent, automated, acid dosing station  
66 built near the original depository. Red mud deposited on the flood plain of the Torna  
67 Creek has been successfully recovered and stored in a newly constructed impoundment  
68 with improved structural integrity (Reeves et al., 2010).

69

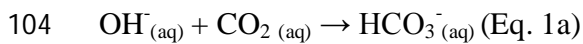
70 Initial studies on the environmental effects of the spill have found that on floodplain soils  
71 inundated with red mud, salinity and high alkalinity rather than contaminant element  
72 enrichment is the key constraint to plant growth (Ruyters et al., 2011), a finding  
73 consistent with the broad body of restoration ecology literature on the rehabilitation of  
74 red mud disposal sites (e.g. Gräfe and Klauber, 2011). Preliminary studies on the fluvial  
75 sediment contamination have highlighted the abundance of vanadium, chromium, nickel  
76 and arsenic downstream of the spill, although the bulk of these potential contaminants  
77 (with the exception of V) appear to be associated principally with hard-to-leach residual  
78 phases that are unlikely to be mobile in the environment (Mayes et al., 2011). The fine  
79 grain size of the released material also lends itself to transport downstream and rapid  
80 dispersion (Mayes et al., 2011). Speciation studies have reinforced these patterns (Burke  
81 et al., 2011), but also highlighted the prevalence of vanadium in mobile pentavalent  
82 species (the most toxic form of V), which may be leached from red mud after deposition  
83 on floodplain areas.

84

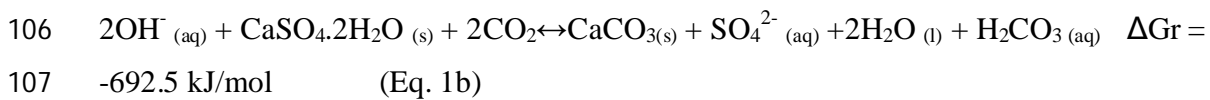
85 Gypsum has been widely used as an ameliorant or soil amendment at bauxite processing  
86 residue (the fine fraction of which is referred to as red mud) disposal sites (e.g. Courtney  
87 et al., 2005; Wehr et al., 2006; Gräfe and Klauber, 2011). The addition of gypsum  
88 provides  $\text{Ca}^{2+}$  which displaces  $\text{Na}^+$  from exchange complexes and reduces salt stress to  
89 vegetation (Gräfe and Klauber, 2011). The  $\text{Ca}^{2+}$  addition also serves to regulate pH and  
90 helps buffer the highly caustic (alkalinity  $>20,000$  mg/L as equivalent  $\text{CaCO}_3$ ; Johnston  
91 et al., 2010) red mud substrate to within the range tolerable by plants (Gräfe and Klauber,  
92 2011). In hyperalkaline conditions, atmospheric  $\text{CO}_2$  readily in-gasses into waters  
93 (Roadcap et al., 2006) and reacts with the hydroxyl ion (abundant in the Bayer liquor

94 from use of NaOH ore digestant) to form bicarbonate (Eq. 1a). The addition of gypsum to  
95 red mud leachate provides free  $\text{Ca}^{2+}$ , prompting precipitation of calcium carbonate (Eq.  
96 1b) which consumes alkalinity and lowers pH (thermodynamic data from Robie and  
97 Hemingway, 1995). Other precipitation products formed through gypsum addition to red  
98 mud slurries include tricalcium aluminate ( $\text{Ca}_3\text{Al}_2\text{O}_6$ ), Portlandite ( $\text{Ca}(\text{OH})_2$ ) and  
99 hydrocalumite ( $\text{Ca}_2\text{Al}(\text{OH})_7 \cdot 2\text{H}_2\text{O}$ ; Gräfe et al., 2011). This buffering process, ubiquitous  
100 in hyperalkaline waters containing the weathering products of portlandite (e.g. steel slag  
101 and some fly ash leachates: Mayes et al., 2009), is otherwise limited in red mud leachates  
102 by the lack of dissolved  $\text{Ca}^{2+}$  and  $\text{Mg}^{2+}$  prior to gypsum addition.

103



105



108

109 Silicate-bearing waste materials may be able to sequester atmospheric  $\text{CO}_2$  on human  
110 relevant time scales at globally significant quantities (Renforth et al., 2011), and red mud  
111 has been suggested to be suitable in this context (Yadav et al., 2010). Existing  
112 investigations of mineral carbonation have shown that the carbon capture potential of a  
113 material is dependent on the quantity of non-carbonated divalent cations (predominantly  
114 Ca and Mg) and the reactivity of the phase in which they are situated. For instance, iron  
115 and steel slags have a typical  $\text{MgO} + \text{CaO}$  content  $>50\%$ , primarily as amorphous glasses,  
116 and have been shown to sequester atmospheric carbon dioxide under ambient  
117 temperatures and  $\text{pCO}_2$  (Renforth et al., 2009).

118

119 Through employing isotopic analyses alongside a range of geochemical investigations,  
120 this paper assesses the efficacy of gypsum dosing as part of emergency management with  
121 regard to the mobility of contaminants downstream of the Ajka red mud spill. The  
122 processes taking place also provide a useful, large-scale analogue to potential remedial  
123 interventions and carbon capture mechanisms at sites managing hyperalkaline slurries  
124 produced in the Bayer Process.

125

126 **Methods**

127 Sediment samples were collected from a series of stations across the 3072km<sup>2</sup> Marcal  
128 river system on the 30<sup>th</sup> November and 1<sup>st</sup> December 2010 (see Mayes et al., 2011 for  
129 detail). At each station triplicate bulk (~500g) sediment samples were collected by  
130 aggregating three randomly collected sub-samples from a 12m<sup>2</sup> area of stream bed (9  
131 separate locations sampled at each reach to give three replicates). Additional spot samples  
132 from stock-piled gypsum deposits (at location M4: Figure 1), gypsum-affected fluvial  
133 sediments (M4), and floodplain deposits of transported red mud at Somlóvásárhely (S1).

134

135 Sediments were homogenized, air-dried, disaggregated gently and sieved (2mm aperture)  
136 prior to microwave-assisted total digestion (aqua regia and HF) following the method of  
137 USEPA (1996). Major and minor element concentrations in digests and extracts were  
138 determined using a Perkin Elmer Elan DRCII inductively Coupled Plasma-Mass  
139 Spectrometer (ICP-MS; for As, Cr and Mo) and an Optima 5300 DV ICP-OES for all  
140 other elements.

141

142 Calcium carbonate content was determined using an Eijkelkamp calcimeter (BS 7755-  
143 3.10:1995). C and O stable isotope ratios were determined on selected samples by Iso-  
144 Analytical Ltd, Crewe, UK (<http://www.iso-analytical.co.uk/>). Carbonate samples were  
145 digested in pure phosphoric acid and isotope ratios were measured on the evolved CO<sub>2</sub>  
146 using a Europa Scientific 20-20 isotope ratio mass spectrometer calibrated against  
147 standards NBS-19, IA-R022 and NBS-18. The mean of the standards was consistently  
148 within one standard deviation of the accepted value and analytical precision was ±0.05 ‰  
149 for δ<sup>13</sup>C and ±0.07 ‰ δ<sup>18</sup>O, referred to Vienna-Pee Dee Belemnite (VPDB).

150

151 Samples of the stockpiled material were analysed using a Netzsch STA449C TG-DSC  
152 (thermogravimetry-differential scanning calorimetry, or TG-DSC) system with an  
153 atmosphere of flowing (30 ml/minute) 80% He, 20% O<sub>2</sub>, in, connected to a Netzsch  
154 Aeolos 403C quadrupole mass spectrometer (QMS; m/z range 10-300). Samples were

155 loaded into alumina crucibles (approximately 30-40 mg sample mass). A heating rate of  
156 10°C min<sup>-1</sup> was used from 0-1000°C.

157

158 Principal Component Analysis and all other statistical analyses were undertaken in  
159 Minitab v15. PCA was undertaken on standardized total extraction data to examine the  
160 evolution of bulk geochemistry with distance from the site and the relative mixing of red  
161 mud with fluvial sediments. Data were not normally distributed even after log-  
162 transformation (Kolmogorov-Smirnov  $p > 0.05$ ) so non-parametric methods were used.  
163 Hydrochemical data from Mayes et al., (2011) and CSIRO (2009) were analysed using  
164 the geochemical code PHREEQC v.1.5.10 (Parkhurst and Apello, 1999) with the  
165 WATEQ4F database (Ball and Nordstrom, 1991).

166

## 167 **Results and Discussion**

### 168 *Trace element attenuation*

169 Bulk elemental analysis of the sediments collected highlights a dilution gradient of red  
170 mud downstream from source areas (rich in Al, Na, As, Cr, Ni, V and rare earth elements:  
171 REE; Table 1) which provide an end-member of the most affected area adjacent to the  
172 cell (K1), to unaffected sites which are relatively enriched in elements indicative of  
173 lithogeneous sources (e.g. Ba, Mg, K; Mayes et al., 2011). Although hotspots of red mud  
174 enrichment are apparent up to around 60-70km downstream of Ajka (e.g. M2, M4) the  
175 signal of red mud deposition is difficult to distinguish from reference sites at sample  
176 stations in lower Marcal (e.g. M7) and those in the Raba (R2) and Mosoni Duna, towards  
177 the confluence with the Danube. The signal of gypsum addition on fluvial sediments is  
178 also stark (Figure 2), with elevated Ca and S relative to source red mud samples and  
179 unaffected sites (Table 1). Total sulphur is a particularly good indicator of gypsum  
180 amendment in the system given theoretical concentrations in gypsum exceeds 186g/kg  
181 while reference sites have total sulphur content between 182 and 552 mg/kg, and source  
182 material (K1) ranges between 2750 and 2894mg/kg. A gradient of mixing from  
183 theoretical gypsum to gypsum-affected stream sediments (e.g. M7, M9-11) is apparent in  
184 the upper left of Figure 2. The addition of gypsum was evident at numerous sample  
185 stations where the streambed was blanketed in gypsum-rich sludges and secondary

186 carbonate precipitates, or where high stage marks on downstream bridge piers suggested  
187 recent carbonate precipitation. These were predominantly on the Marcal river, but  
188 stations at K3, T3 and T6 on the Torna Creek also exhibit elevated S concentrations  
189 elevated above impoundment samples and reference samples suggesting significant  
190 localised gypsum addition (Table 1; Figure 2).

191 Analysis of the gypsum-amended instream sediments suggests some modest trace  
192 element uptake relative to adjacent stockpiled samples (Table 2). For some of the more  
193 mobile elements downstream of the impoundment (As, Cr, V: see Mayes et al., 2011) this  
194 difference is statistically significant, albeit obtained from a small sample size. Whether  
195 this reflects uptake of such elements within secondary deposits and gypsum, or capture of  
196 colloidal red mud fines transported downstream of the site is uncertain. Sequential  
197 extraction of affected fluvial sediments at the site suggested a greater relative importance  
198 of NaOAc / HOAc and NH<sub>2</sub>OH.HCl extractable phases (in the operationally defined  
199 Tessier et al. (1979) scheme) of As, Ni and V at sites subject to gypsum dosing than  
200 source sediments (Mayes et al. 2011). This could support the notion of scavenging by  
201 gypsum and neo-formed carbonate deposits but further analysis would be required to  
202 elucidate specific modes of attenuation. It should be noted that due to the potential  
203 precipitation of CaF<sub>2</sub> during aqua regia-HF acid digestion, the accuracy of the values  
204 reported for Ca in Table 1 is limited. For this reason, total S concentration has been used  
205 to understand gypsum addition in the catchment.

206

#### 207 *Stockpiled Gypsum Analysis*

208 The purity of the stockpiled gypsum was confirmed using thermogravimetric analysis in  
209 which a 15-18% mass loss was recorded at 150°C which is indicative of gypsum  
210 dehydration. Varying weight loss (3-7%) was recorded at 700°C, indicative of calcium  
211 carbonate decarbonation. This suggests that the sample is approximately 71-86% gypsum  
212 and 7-16% calcium carbonate. X-ray diffraction analysis (XRD) confirmed that gypsum  
213 and calcite are the predominant phases in the sample.

214

#### 215 *Stable isotope data*

216 C and O stable isotope ratios in carbonates have been used to investigate the provenance  
 217 of the elemental components and the condition of the environment from which they form  
 218 (e.g. Hudson, 1977). There is a distinctive isotopic composition in carbonates formed  
 219 from high pH solutions associated with waste silicate materials such as cement (Dietzel et  
 220 al., 1992; Krishnamuthy et al., 2003; Macleod et al., 1991), lime waste (Andrews, 1997),  
 221 iron and steel slag (Renforth et al., 2009) and ashes (Fléhoc et al., 2006; see Figure 3).  
 222 The light  $\delta^{13}\text{C}$  isotopic signatures are explained using the interpretation proposed by  
 223 Uzdowski and Hoefs (1986), who suggest an isotopic enrichment factor of  $\delta^{13}\text{C}$  (Eq 2) in  
 224 carbonate and dissolved  $\text{CO}_2$  during the reaction shown in Eq 1a.

225

$$226 \quad \epsilon_{\text{CaCO}_3\text{-CO}_2} = -18.8 \text{ ‰} \quad (\text{Eq. 2})$$

227

228 The carbonate mineral  $\delta^{18}\text{O}$  in high pH solutions is a mixture of  $\delta^{18}\text{O}$  produced from the  
 229 fractionation between hydroxide and meteoric water, and atmospheric  $\text{CO}_2$  according to  
 230 Equations 3 and 4 (Dietzel et al., 1992; Uzdowski and Hoefs, 1986; Letolle et al., 1990):

231

$$232 \quad \delta^{18}\text{O}_{\text{CaCO}_3} = \frac{1}{3} \delta^{18}\text{O}_{\text{OH}^-} + \frac{2}{3} \delta^{18}\text{O}_{\text{CO}_2} \quad (\text{Eq. 3})$$

$$233 \quad \epsilon_{\text{OH}^- \text{-H}_2\text{O}} = -42 \text{ ‰} \quad (\text{Eq. 4})$$

234

235 This is generally consistent with the low O isotope ratios reported in the literature  
 236 (Andrews et al., 1997; Clark et al., 1992; Fléhoc et al., 2006; Kosednar-Legenstein et al.,  
 237 2008; Krishnamurthy et al., 2003; Macleod et al., 1991; O'Neil and Barnes, 1971;  
 238 Renforth et al., 2009; van Strydonck et al., 1989). The influence of atmospheric carbon  
 239 and  $\epsilon_{\text{OH}^- \text{-H}_2\text{O}}$  in Equations 3 and 4 reduces the effect of  $\delta^{18}\text{O}$  meteoric water variation  
 240 between -50 and -35 ‰ to precipitate carbonates in high pH solutions with  $\delta^{18}\text{O}$  between  
 241 a smaller range of -24 and -19 ‰. This approach provides a useful tool in highlighting the  
 242 importance of secondary carbonates as a carbon sink.

243

244 Carbonate stable isotope ratios were  $-12.80 \text{ ‰} \leq \delta^{13}\text{C} \leq -3.54\text{‰}$ , and  $-12.37 \text{ ‰} \leq \delta^{18}\text{O} \leq -$   
 245  $8.03\text{‰}$ . Isotope ratios were more negative adjacent to the storage facility (points K3, S1  
 246 and T1 had  $\delta^{13}\text{C}$  between  $-10.90\text{‰}$  and  $-12.40\text{‰}$ , and  $\delta^{18}\text{O}$  between  $-10.38\text{‰}$  and -

247 12.37‰). In contrast, carbonate isotope ratios adjacent to the confluence between the  
248 Mosoni-Duna and the Danube (MD1 and R2) are more consistent with those in the  
249 Triassic limestone bedrock ( $\delta^{13}\text{C} = -3.5\text{‰}$ ,  $\delta^{18}\text{O} = -1.7\text{‰}$ ; Pálffy et al., 2001)

250

251 Assuming that atmospheric  $\text{CO}_2$  is the only source of carbon in hydroxylation isotopic  
252 fractionation, the proximity of the isotope values in the samples to end members can be  
253 used to determine the quantity of sequestered atmospheric  $\text{CO}_2$ . Hydroxylation will  
254 produce an end member with an isotopic ratio of  $-27.0\text{‰}$  for  $\delta^{13}\text{C}$ , and  $-20.0\text{‰}$  for  $\delta^{18}\text{O}$   
255 (assuming meteoric water  $-37.5\text{‰} \leq \delta^{18}\text{O} \leq -35.2\text{‰}$ ; Bajnóczi and Kovács-Kis, 2006).  
256 Therefore, it is estimated that between 10.5 and  $38.1 \pm 0.6\%$  of the carbon in the carbonate  
257 is derived from the atmosphere and the remaining carbonate is derived from lithogenic  
258 sources (Table 3).

259

260 There is a strong, significant positive correlation ( $r_s = 0.94$ ;  $p = 0.005$ ) between total S  
261 content of the sample and the proportion of carbon derived through hydroxylation of  
262 atmospheric  $\text{CO}_2$  (Figure 4). This suggests the greater influence of secondary carbonate  
263 deposits at the heavily gypsum-dosed sites, as would be anticipated given the addition of  
264 non-carbonated divalent cations (notably  $\text{Ca}^{2+}$ ,  $\text{Mg}^{2+}$  and  $\text{Sr}^{2+}$ ; Table 1). The relationship  
265 does not reflect the downstream gradient in pH that was apparent shortly after the spill  
266 (ECMICCP, 2010) or the sharper pH gradient from residual releases in the months after  
267 (Mayes et al., 2011). While there are samples with a high proportion of atmospheric  
268 carbon in the deposits in source areas (e.g. K3, T1), and the lowest proportion towards the  
269 largely unaffected sites at the catchment outlet (R2, MD1), there is a particular hotspot of  
270 gypsum enrichment (and enhanced carbonate crust formation indicative of atmospheric  
271 sources) at site M11. This site lies around 15km downstream of a temporary gypsum  
272 storage depot which was a focus for coordinating dosing efforts in the spill aftermath at  
273 Mórchida (Hungarian Foreign Affairs Ministry, 2010) and was particularly gypsum-rich.  
274 Sample S1 (transported red mud) has relatively elevated S, reflecting the influence of the  
275 source term (Table 1), while the relative elevation of the atmospherically-derived carbon  
276 at the transported red mud sample S1 may reflect the carbonation apparent in surface  
277 deposited red mud which gets at least partially neutralised over time (Gräfe et al., 2011).

278

279

### 280 *PHREEQC Modelling Results*

281 To understand the effect of gypsum addition on the saturation state of carbonate minerals  
282 in red mud leachate solutions, a model was constructed in PHREEQC using solution  
283 chemistry data from Mayes et al., (2011) for sample points K1, K2 and K3 and laboratory  
284 leaching results (CSIRO, 2009), which are indicative of solutions in contact with red  
285 mud. The results (Table 4) show that solutions in equilibrium with gypsum are more  
286 saturated with respect to calcite and aragonite. While solution pH is directly reduced by  
287 gypsum addition as seen in Table 4, carbonate precipitation (resulting in the dissolution  
288 of additional CO<sub>2</sub> and the deprotonation of H<sub>2</sub>CO<sub>3</sub>) is probably the key pH reduction  
289 mechanism in the environment which is not shown in static equilibrium models.

290

### 291 **Conclusions and management implications**

292 The acid neutralising capacity of red mud is approximately 10 mol/kg, equivalent to a  
293 reduction in [H<sup>+</sup>] or an increase in [OH<sup>-</sup>]. Equation 1 suggests that 1 mole of gypsum is  
294 required to neutralise 2 moles of OH<sup>-</sup> and form 1 mole of CaCO<sub>3</sub>. Therefore, every tonne  
295 of red mud requires approximately 860kg of gypsum, which would capture  
296 approximately 220kg of CO<sub>2</sub>. Between 60-120 Mt of red mud is produced annually  
297 (Ruyters et al., 2011; Yadav et al., 2010; Liu et al., 2007), which could be treated with  
298 52-103 Mt of gypsum (33-69% of current global crude and synthetic gypsum production;  
299 USGS 2010) and sequester 13-26 Mt of CO<sub>2</sub> (3-4% of CO<sub>2</sub> emissions from primary  
300 aluminium production; (Harnisch et al., 1998; USGS 2011). The global inventory of red  
301 mud may be approximately 2600Mt (Power et al., 2011), which may have a carbon  
302 capture potential of 572 Mt CO<sub>2</sub>. The large scale extraction, processing, and transport of  
303 gypsum is indicative of other carbon reduction geoengineering technologies (see The  
304 Royal Society, 2009) and may be coupled to the desulphurisation process on coal fired  
305 power stations as has been successfully deployed elsewhere (e.g. Yamada and Harado,  
306 1982; Leoni and Penco, 2002). However, a comprehensive cost benefit analysis, which  
307 includes the reduced risk of contamination, is required to assess the feasibility of treating

308 red mud in this way. This gypsum dosing method may be suitable for other industries  
309 with NaOH bearing waste streams including ‘black liquor’ in paper manufacturing,

310

311 Gypsum has been widely applied in ameliorating the high alkalinity of bauxite residue  
312 slurries and solids (Courtney et al., 2005; Gräfe et al., 2011). The emergency  
313 management in the aftermath of the Ajka spill represents the largest-scale field  
314 application of gypsum to red mud leachate-affected surface waters. The gypsum dosing  
315 was deemed effective in buffering the high pH waters after the initial release (Hungarian  
316 Ministry of Foreign Affairs, 2010) and secondary deposits have sequestered both trace  
317 contaminants and atmospheric carbon in demonstrable quantities. Gypsum is also  
318 currently being used in new waste stockpiling and stabilisation procedures at Ajka  
319 (Benedek, 2011). As such, gypsum addition may represent an avenue for future  
320 experimentation under controlled conditions to develop long-term buffering alternatives  
321 to direct acid neutralisation. Other buffering alternatives, such as direct carbonation  
322 (which suffers from transient buffering effects; Khaitan et al., 2009) and microbial  
323 buffering (see Gräfe et al., 2011 for detail) represent other means to develop sustainable  
324 treatment technologies for hyperalkaline red mud leachates, particularly at disposal sites  
325 in temperate climate zones where leachate generation can pose an enduring problem and  
326 acid dosing is not economically viable over the long term. However, the broader  
327 ecological effects of gypsum addition may warrant further investigation. In analogous  
328 systems receiving hyperalkaline calcareous waters, numerous deleterious effects have  
329 been noted. These include (1) the effects of extensive benthic smothering and rapid rates  
330 of carbonate deposition (e.g. Koryak et al., 2002), (2) poor physical structure of  
331 secondary calcareous deposits (Auer et al., 1996; Madsen et al., 1996) and (3) the  
332 formation of hardpans, which prevent root penetration under low flow conditions (Mayes  
333 et al. 2009).

334

### 335 **Acknowledgements**

336 We are grateful to the UK Natural Environment Research Council for funding the work (grant  
337 NE/I019468/1). We are indebted to Bob Knight (University of Hull) and Jane Davis (Newcastle University)  
338 for analyses. We also thank Viktória Feigl, Orsolya Klebercz, Mária Tolner, Ermese Vaszita (Budapest  
339 University of Technology and Economics) for field support; Gyozo Jordan (Geological Institute of

340 Hungary), Kovacs Laszlo and István Csonki (Central Danubian Water and Environment Authority) for site  
341 information; and Krisztina Kocsis (British Embassy) for facilitating site access. We would like to thank  
342 Markus Gräfe and an anonymous reviewer for insightful comments that have improved the manuscript.  
343

## 344 **References**

- 345 Andrews, J. E.; Gare, S. G.; Dennis, P. F. Unusual isotopic phenomena in Welsh quarry water and  
346 carbonate crusts. *Terra Nova*, 1997; 9: 67-70.
- 347 Auer, M.T.; Johnson, N.A.; Penn, M.R.; Effler, S.W. Pollutant sources, depositional environment and the  
348 surficial sediments of Onondaga Lake, New York. *Journal of Environmental Qual.* 1996; 25: 46-55.
- 349 Bajnóczi, B., Kovács-Kis, V. Origin of pedogenic needle-fiber calcite revealed by micromorphology and  
350 stable isotope composition--a case study of a Quaternary paleosol from Hungary. *Chemie der Erde -*  
351 *Geochemistry*, 2006; 66: 203-212.
- 352 Ball, J.W.; Nordstrom, D.K. User's Manual for WATEQ4F with Revised Thermodynamic Database and  
353 Test Cases for Calculating Speciation of Major, Trace and Redox Elements in Natural Waters, U.S.  
354 Geological Survey Water Resources Investigation, Report 91-183. 1991.
- 355 Benedek, J. (ed). *The Kolontár Report: Causes and Lessons from the Red Mud Disaster*. Sustainable  
356 Development Committee of the Hungarian Parliament. Budapest. 2011.
- 357 Burke, I.T., Mayes, W.M., Peacock, C.L., Brown, A.P., Jarvis, A.P., Gruiz, K. Speciation of contaminant  
358 metals in red mud samples from the Ajka spill site, Hungary. *Mineralogical Magazine*, 2011;  
359 75(3):599.
- 360 CSIRO, *Characterisation of Mining and Industrial By-Products with Potential for Use as Environmental*  
361 *Amendments*. Western Australia Water Foundation. ISSN: 1835-095X. 2009
- 362 Clark, I.D.; Fontes, J-C.; Fritz, P. Stable isotope disequilibria in travertine from high pH waters: Laboratory  
363 investigations and field observations from Oman. *Geochimica et Cosmochimica Acta*, 1992; 56: 2041-  
364 2050.
- 365 Courtney, R.G.; Timpson, J.P. Reclamation of fine fraction bauxite processing residue (red mud) amended  
366 with coarse fraction residue and gypsum. *Water, Soil, Air Pollut.* 2005; 164: 91-102.
- 367 Dietzel, M.; Usdowski, E.; Hoefs, J. Chemical and <sup>13</sup>C/<sup>12</sup>C- and <sup>18</sup>O/<sup>16</sup>O-isotope evolution of alkaline  
368 drainage waters and the precipitation of calcite. *Applied Geochemistry*, 1992; 7:177-184.
- 369 European Commission Monitoring and Information Centre for Civil Protection. *Alkali Sludge Depository*  
370 *Dyke Breach in Kolontár, Veszprém County, Hungary Situation Report 3*. European Union, October  
371 6<sup>th</sup>, 2010.
- 372 Fléhoc, C.; Girard, J.P.; Piantone, P.; Bodénan, F. Stable isotope evidence for the atmospheric origin of  
373 CO<sub>2</sub> involved in carbonation of MSWI bottom ash. *Applied Geochemistry*, 2006; 21:2037-2048.
- 374 Gelencsér, A.; Kováts, N.; Turóczy, B.; Rostási, Á.; Hoffer, A.; Imre, K.; Nyirő-Kósa, I.; Csákberényi-  
375 Malasics, D.; Tóth, Á.; Czitrovsky, A.; Nagy, A.; Nagy, S.; Ács, A.; Kovács, A.; Ferincz, Á.; Hartyáni,

376 Z.; Pósfai, M. The red mud accident in Ajka (Hungary): characterization and potential health effects of  
377 fugitive dust. *Environ. Sci. Technol.* 2011. 45:1608-1615.

378 Gräfe, M., Klauber, C. Bauxite residue issues: IV. Old obstacles and new pathways for in-situ  
379 bioremediation. *Hydrometallurgy*. 2011; 108:46-59.

380 Gräfe, M., Power, G., Klauber, C. Bauxite residue issues: III. Alkalinity and associated chemistry.  
381 *Hydrometallurgy*. 2011; 108:60-79.

382 Gruiz, K. Environmental Information: The red mud catastrophe in Hungary.  
383 [http://enfo.agt.bme.hu/drupal/en/gallery/8081\\_2010](http://enfo.agt.bme.hu/drupal/en/gallery/8081_2010). 2010.

384 Harnisch, J., I., Sue Wing, H.D. Jacoby and R.G. Prinn, Primary aluminum production: Climate policy,  
385 emissions and costs, MIT JPSPGC Report No. 44, December  
386 (<http://web.mit.edu/globalchange/www/rpt44.html>); also Extraction and Processing Division Congress  
387 1999, The Minerals Metals and Materials Society. 1998.

388 Hudson, J.D., Stable isotopes and limestone lithification. *Journal of the Geological Society*, 1977;:  
389 133(6):637-660.

390 Hungarian Ministry of Foreign Affairs. Information on the accidental pollution and related mitigation  
391 measures of the “red mud spill at Ajka”  
392 [http://www.mfa.gov.hu/kulkepvisolet/CZ/en/en\\_Hirek/V%C3%B6r%C3%B6siszap\\_en.htm?printable=](http://www.mfa.gov.hu/kulkepvisolet/CZ/en/en_Hirek/V%C3%B6r%C3%B6siszap_en.htm?printable=true)  
393 [true](http://www.mfa.gov.hu/kulkepvisolet/CZ/en/en_Hirek/V%C3%B6r%C3%B6siszap_en.htm?printable=true) [ last accessed: 07.07.2011] 2010.

394 Johnston, M.; Clark, M.; McMahon, P.; Ward, N. Alkalinity conversion of bauxite refinery residues by  
395 neutralization. *J.Hazard. Mater.* 2010; 182:710-715.

396 Khaitan S.; Dzombak D.A.; Lowry G.V. Neutralization of bauxite residue with acidic fly ash. *Environ.*  
397 *Eng. Sci.* 2009; 26:431-440.

398 Koryak, M.; Stafford, L.J.; Reilly, R.J.; Magnuson, M.P. Impacts of steel mill slag leachate on the water  
399 quality of a small Pennsylvania stream. *Journal of Freshwater Ecology*, 2002; 17:461-465.

400 Kosednar-Legenstein, B.; Dietzel, M.; Leis, A.; Stingl, K. Stable carbon and oxygen isotope investigation  
401 in historical lime mortar and plaster - Results from field and experimental study. *Applied*  
402 *Geochemistry*, 2008; 23:2425-2437.

403 Krishnamurthy, R.V.; Schmitt, D.; Atekwana, E.A.; Baskaran, M. Isotopic investigations of carbonate  
404 growth on concrete structures. *Applied Geochemistry*, 2003; 18:435-444.

405 Leoni, F. & Penco, C. Bauxite residue desulphurisation system (BRDS) at Eurallumina. in Chandrashekar,  
406 S. (Ed.) *Proceedings of the 6th International Alumina Quality Workshop, Brisbane, AQW Inc.* 2002.

407 Létolle, R.; Gégout, P.; Moranville-Regourd, M.; Gaveau, B. Carbon-13 and oxygen-18 mass spectrometry  
408 as a potential tool for the study of carbonate phases in concretes. *Journal of the American Ceramic*  
409 *Society*, 1990; 73:3617-3625.

410 Liu, Y., C. Lin, and Y. Wu, Characterization of red mud derived from a combined Bayer Process and  
411 Calcining method for alumina refining. *Chinese Journal of Geochemistry*, 2007. 25(0):40-40.

412 Macleod, G., Fallick, A. E. & Hall, A. J. The mechanism of carbonate growth on concrete structures, as  
413 elucidated by carbon and oxygen isotope analyses. *Chemical Geology*, 1991; 86:335-343.

414 Madsen, J.D.; Bloomfield, J.A.; Sutherland, J.W.; Eichler, L.W.; Boylen, C.W. The aquatic macrophyte  
415 community of Onondaga Lake: Field survey and plant growth bioassays of lake sediments. *Lake and*  
416 *Reservoir Management*, 1996; 12:73-79.

417 Mayes W.M.; Batty, L.C.; Younger, P.L.; Jarvis, A.P.; Kőiv, M.; Vohla, C.; Mander, Ü. Wetland treatment  
418 at extremes of pH – a review. *Sci. Total Environ.* 2009; 407:3944-3957.

419 Mayes, W.M.; Jarvis, A.P.; Burke, I.T., Walton, M.; Feigl, V; Klebercz, O.; Gruiz, K. Dispersal and  
420 attenuation of trace contaminants downstream of the Ajka bauxite residue (red mud) depository failure,  
421 Hungary. *Environ. Sci. Technol.* 2011; 45:5147-5155.

422 O'Neil, J. R. & Barnes, I. C<sup>13</sup> and O<sup>18</sup> compositions in some fresh-water carbonates associated with  
423 ultramafic rocks and serpentinites: western United States. *Geochim. Cosmochim. Act.*, 1971; 35: 687-  
424 697.

425 Pálffy, J.; Demény, A.; Haas, J.; Hetényi, M.; Orchard, M.J.; Veto, I. Carbon isotope anomaly and other  
426 geochemical changes at the Triassic-Jurassic boundary from a marine section in Hungary. *Geology*,  
427 2001; 29:1047-1050.

428 Parkhurst, D.L.; Appelo, C.A.J. User's guide to PHREEQC--A computer program for speciation, batch-  
429 reaction, one-dimensional transport, and inverse geochemical calculations. U.S. Geological Survey  
430 Water-Resources Investigations Report 99-4259. 1999.

431 Power, G; Gräfe, M; Klauber, C. (2011) Bauxite residue issues: I. Current management, disposal and  
432 storage practices. *Hydrometallurgy*. 2011; 108:33-45.

433 Reeves, H.J.; Wealthall, G.; Younger, P.L. Advisory visit to the bauxite processing tailings dam near Ajka,  
434 Veszprém County, western Hungary. British Geological Survey, Keyworth, UK. Open Report  
435 OR/11/006. 2011.

436 Renforth, P.; Manning, D.A.C.; Lopez-Capel, E. Carbonate precipitation in artificial soils as a sink for  
437 atmospheric carbon dioxide. *Applied Geochemistry*, 2009; 24:1757-1764.

438 Renforth, P.; Washbourne, C. L.; Taylder, J.; Manning, D.A.C. Silicate Production and Availability for  
439 Mineral Carbonation. *Environ. Sci. Technol.* 2011; 45:2035-2041.

440 Roadcap, G. S.; Kelly, W. R.; Bethke, C. M. Geochemistry of extremely alkaline (pH>12) ground water in  
441 slag-fill aquifer. *Ground Water*, 2005; 43:806-816.

442 Robie, R. A., Hemingway, B. S. Thermodynamic properties of minerals and related substances at 298.15 K  
443 and 1 bar (105 Pascals) pressure and at higher temperatures. In United States Geological Survey  
444 Bulletin 2131; WA, 1995.

445 Ruyters, S.; Mertens, J.; Vassilieva, E.; Dehandschutter, B.; Poffijn, A.; Smolders, E. The red mud accident  
446 in Ajka (Hungary): Plant toxicity and trace metal bioavailability in red mud contaminated soil.  
447 *Environ. Sci. Technol.* 2011; 45:1616-1622.

448 Tessier, A.; Campbell, P.G.C.; Bisson, M. Sequential extraction procedure for the speciation of particulate  
449 trace metals. *Anal. Chem.* 1979; 51:844-851.

450 The Royal Society. *Geoengineering the Climate: Science, governance and uncertainty*. The Royal Society:  
451 London, UK, 2009

452 Usdowski, E.; Hoefs, J.  $^{13}\text{C}/^{12}\text{C}$  partitioning and kinetics of  $\text{CO}_2$  absorption by hydroxide buffer  
453 solutions. *Earth and Planetary Science Letters*, 1986; 80:130-134.

454 USEPA. Microwave assisted acid digestion of siliceous and organically based matrices. Method 2052.  
455 1996.

456 USGS. *United States Geophysical Survey Minerals Yearbook*. U.S. Department of the Interior and U.S.  
457 Geological Survey. 2010.

458 USGS. *United States Geophysical Survey Minerals Commodity: Aluminium*, U.S. Department of the  
459 Interior and U.S. Geological Survey. 2011. (Available at  
460 <http://minerals.usgs.gov/minerals/pubs/commodity/aluminum/mcs-2011-alumi.pdf>)

461 Van Strydonck, M.J.Y.; Dupas, M; Keppens, E. Isotopic fractionation of oxygen and carbon in lime mortar  
462 under natural environmental conditions. *Radiocarbon*. 1989; 31:610-618.

463 Wehr, J.B.; Fulton, I.; Menzies, N.W. Revegetation strategies for bauxite refinery residue: a case study of  
464 Alcan Gove in Northern Territory, Australia. *Environ. Management*. 2006; 37:297-306.

465 Yadav, V. S.; Prasad, M.; Khan, J.; Amritphale, S. S.; Singh, M; Raju, C. B. Sequestration of carbon  
466 dioxide ( $\text{CO}_2$ ) using red mud. *J.Hazard. Mater.*, 2010; 176:1044-1050.

467 Yamada, K.; Harato, F.  $\text{SO}_2$  removal from waste-gas by red mud slurry pilot test and operation results of  
468 the plant. *Kagaku Kogaku Ronbunshu*; 1982; 8:32-38

469  
470  
471  
472  
473  
474  
475  
476  
477  
478  
479  
480  
481  
482  
483  
484  
485  
486  
487  
488  
489

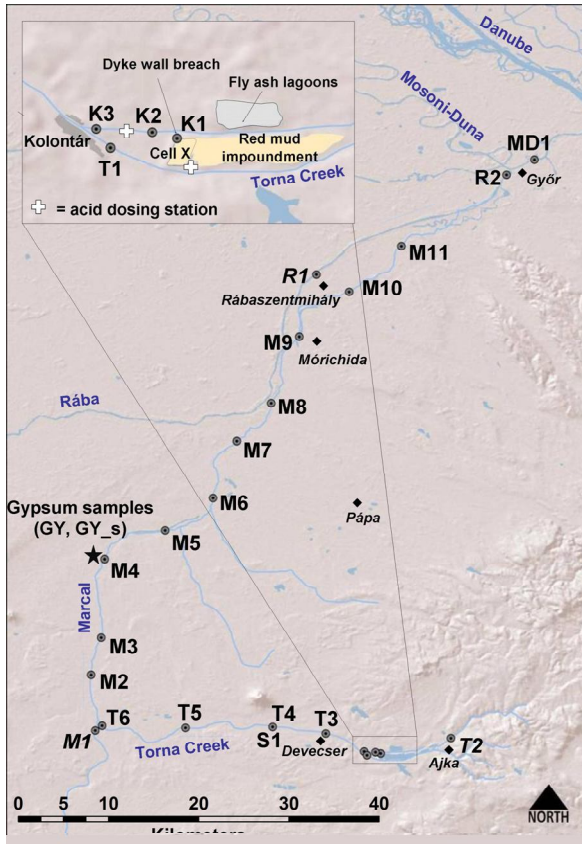
490 **Figure Legends**

491

492 Figure 1. Location map of sample stations (circles) across the Marcal and Rába catchments.

493 Population centres shown with a diamond. Reference site labels in italics.

494



495

496

497

498

499

500

501

502

503

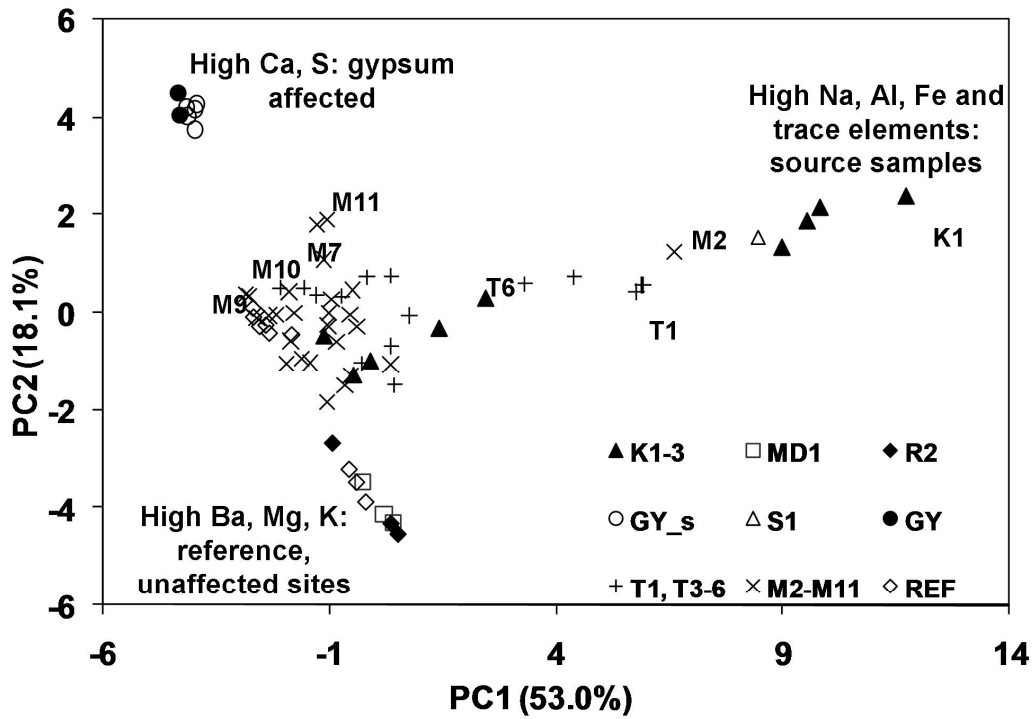
504

505

506

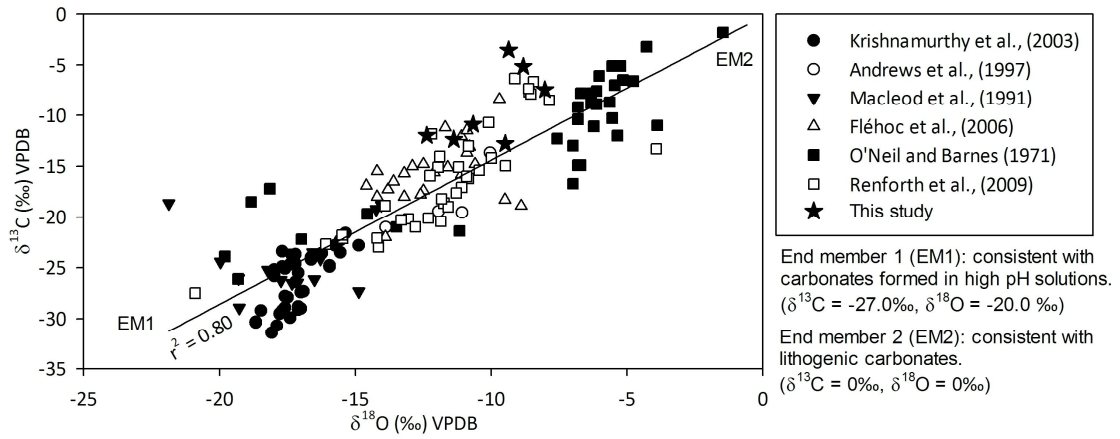
507

508 Figure 2. Principal Component Analysis of sediment total elemental composition data by site  
 509 (after Mayes et al., 2011). Ordination of sample sites by the first two principal components is  
 510 displayed. GY: stockpiled gypsum; GY\_s: instream gypsum deposits; S1: floodplain sample  
 511 adjacent to T4.



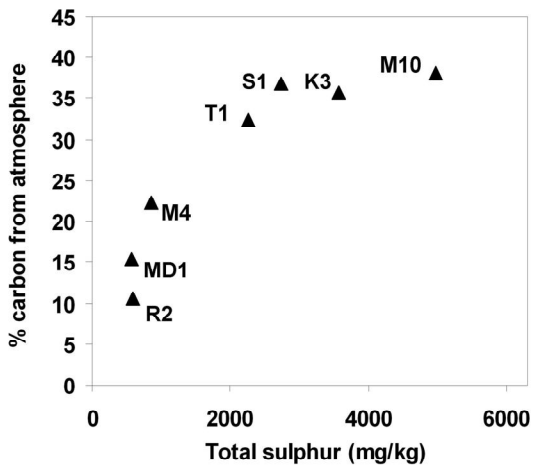
512  
 513  
 514  
 515  
 516  
 517  
 518  
 519  
 520  
 521  
 522

523 Figure 3: Isotopic ratios of carbonates formed in high pH environments. The line denotes linear  
 524 mixing of carbonates between hydroxylation and lithogenic carbonate end members. Analytical  
 525 error is within the size of the data points.



526  
 527

528 Figure 4. Total sulphur content (mean of 3 samples) versus the proportion of carbon estimated to  
 529 be derived from hydroxylation of atmospheric carbon.



530  
 531  
 532  
 533  
 534  
 535  
 536  
 537  
 538  
 539  
 540  
 541

542 **Tables**

543

544 Table 1. Mean composition of digested (aqua regia/HF) fluvial sediments ( $n=3$ ) at selected  
 545 sample stations on the Torna Creek and Marcal River (after Mayes et al., 2011). All values in  
 546 mg/kg. Reference samples M1, R1 and T2 shown on right hand side (italics). S1: floodplain  
 547 deposit from Somlóvásárhely; G: stoichiometric concentrations of Ca and S in pure gypsum.

548

549

Element	K1	K3	T1	S1	M4	M7	M10	<i>M1</i>	<i>R1</i>	<i>T2</i>	<i>G</i>
Distance from spill (km)	0	1.5	1.6	9.4	44.7	64.2	85.9	25.8	100.0	-6.3	44.7
Ca	53500	79100	79900	47900	73000	135000	81300	17000	10400	40400	232600
Mg	2982	7111	8733	3674	7718	19100	7370	3859	8351	10530	-
K	737	5543	5476	2637	5239	5758	9119	8166	18662	9235	-
Na	39920	19390	21980	43220	26120	2969	4401	5350	9760	9522	-
Fe	210300	113500	141600	174400	29300	11100	16400	11100	34800	13100	-
Al	75200	56300	59600	65300	59000	54900	37300	22800	66500	27300	-
Si	27900	75900	65000	47700	66000	113000	184700	339300	165200	54700	-
S	2692	3050	2262	2545	861	3887	4965	155	458	139	186000
As	78.5	51.9	54.3	61.3	52.8	45.4	14.9	5.8	3.1	1.7	-
Ba	59.8	168.4	134.3	52.0	121.7	189.2	203.4	183.7	448.3	163.9	-
Cd	4.0	1.7	2.1	2.7	2.0	1.6	<1	<1	<1	<1	-
Ce	473.2	254.8	264.8	422.5	285.4	7.3	17.8	25.5	54.2	27.5	-
Co	97.1	52.4	54.1	85.3	58.0	6.1	9.1	6.0	10.2	8.5	-
Cr	810.7	372.6	422.6	592.8	416.3	27.7	37.3	30.3	49.2	29.2	-
Cu	60.3	42.6	40.5	47.6	40.1	21.2	21.9	9.3	25.4	15.1	-
Ga	79.3	52.9	53.4	69.0	54.7	39.6	33.7	8.9	27.3	13.0	-
Li	57.5	60.5	54.9	65.3	58.6	20.9	23.0	12.7	40.9	13.6	-
Mn	2565.8	1606.8	1538.7	2462.3	1702.0	1855.3	1327.0	292.8	976.5	420.8	-
Mo	14.4	7.3	10.1	11.2	9.5	10.6	10.3	7.7	5.0	5.4	-
Ni	291.7	140.7	153.5	246.0	162.5	12.3	19.2	12.5	33.5	7.6	-
Pb	79.8	39.6	41.0	68.1	44.1	2.8	4.9	1.3	<1	2.6	-
Sr	290.2	235.0	246.7	299.1	256.4	335.9	204.1	91.5	100.6	124.3	-
Ti	24800	12400	15000	21500	3721	1009	1557	1692	4718	3665	-
V	891.2	458.9	488.3	743.2	510.3	133.7	86.1	28.9	65.9	34.4	-
Zn	173.2	104.3	112.0	132.0	108.8	50.7	77.4	26.3	93.8	26.6	-
Zr	628.9	323.1	341.4	531.8	360.2	13.8	22.3	18.4	37.0	35.1	-

550

551

552

553

554

555

556

557

558 Table 2. Median and range (in parenthesis) in selected major and minor element  
 559 concentrations (mg/kg) in stockpiled gypsum and gypsum-amended fluvial sediments  
 560 taken from sample location M4 (n = 6 for stockpiled gypsum, n = 7 for secondary  
 561 deposits; \*indicates median is significantly higher at  $p < 0.05$  using Mann Whitney U  
 562 test).

563

Site	As	Cr	Cu	Mn	Ni	S	V	Zn
Stockpiled gypsum	13.3 (10.0-28.5)	3.7 (2.8-5.2)	3.0 (1.7-4.1)	16.0 (6.0-27.4)	1.9 (1.0-5.5)	235300* (152300-248100)	2.3 (1.1-3.5)	7.5 (4.4-9.2)
Secondary in-stream calcareous deposits	31.5* (12.5-45.0)	6.4* (4.1-14.4)	2.4 (1.7-5.22)	54.3* (18.6-106.4)	2.9 (1-7.8)	151800 (123100-223800)	4.9* (3.2-19.6)	9.7 (3.1-18.5)

564

565

566

567 Table 3. Isotopic ratios of samples and % of carbon derived from the atmosphere

568

Sample	Distance from source (km)	$\delta^{13}\text{C}_{\text{V-PBD}}$ (‰)	$\delta^{18}\text{O}_{\text{V-PBD}}$ (‰)	% Carbon from the atmosphere (based on carbon isotope ratios)
<b>K3</b>	1.5	-12.00	-12.37	35.7
<b>T1</b>	1.6	-10.90	-10.67	32.4
<b>S1</b>	9.4	-12.40	-11.38	36.9
<b>M4</b>	44.7	-7.48	-8.03	22.2
<b>M10</b>	85.9	-12.80	-9.49	38.1
<b>R2</b>	105.5	-3.54	-9.36	10.5
<b>MD1</b>	110.0	-5.17	-8.82	15.4

569

570

571

572

573

574 Table 4: PHREEQC model input/output of red mud solution chemistry reported (R) in  
 575 Mayes et al. (2011) and CSIRO (2009) and after the solution is modelled in equilibrium  
 576 with gypsum (G).

	Mayes et al., (2011)						CSIRO (2009)	
	K1 -R	K1 -G	K2 -R	K2 -G	K3 -R	K3 -G	R	G
<b>pH</b>	13.06	12.88	10.50	10.29	10.08	9.86	10.66	10.20
<b>Temp</b> (°C)	3.60		4.20		3.90		20.00	
	$\mu\text{mol l}^{-1}$							
<b>Ca</b>	37.82	18510	2.22	13820	0.94	13780	47.48	19100
<b>SO<sub>4</sub></b>	7.57	18480	2.95	13820	2.71	13780	1772	20830
<b>SI</b>	-5.74	0.00	-6.63	0.00	-7.03	0.00	-3.59	0.00
<b>Gypsum</b>								
<b>SI</b>	-1.46	0.53	-2.99	-0.28	-3.50	-0.30	0.62	2.77
<b>Aragonite</b>								
<b>SI Calcite</b>	-1.29	0.69	-2.83	-0.12	-3.34	-0.14	0.77	2.92

577

578